The Astrophysical Journal Letters, 753:L19 (4pp), 2012 July 1 doi:10.1088/2041-8205/753/1/L19

THE SLOW-MODE NATURE OF COMPRESSIBLE WAVE POWER IN SOLAR WIND TURBULENCE

G. G. Howes[1], S. D. Bale[2,3], K. G. Klein[1], C. H. K. Chen[2], C. S. Salem[2], and J. M. TenBarge[1]
[1] Department of Physics and Astronomy, University of Iowa, Iowa City, IA 52242, USA
[2] Space Sciences Laboratory, University of California, Berkeley, CA 94720-7450, USA
[3] Department of Physics, University of California, Berkeley, CA 94720-7300, USA
Received 2011 September 15; accepted 2012 June 1; published 2012 June 15

ABSTRACT

We use a large, statistical set of measurements from the *Wind* spacecraft at 1 AU, and supporting synthetic spacecraft data based on kinetic plasma theory, to show that the compressible component of inertial range solar wind turbulence is primarily in the kinetic *slow* mode. The zero-lag cross-correlation $C(\delta n, \delta B_\parallel)$ between proton density fluctuations δn and the field-aligned (compressible) component of the magnetic field $\delta B_\parallel$ is negative and close to -1. The typical dependence of $C(\delta n, \delta B_\parallel)$ on the ion plasma beta β_i is consistent with a spectrum of compressible wave energy that is almost entirely in the kinetic slow mode. This has important implications for both the nature of the density fluctuation spectrum and for the cascade of kinetic turbulence to short wavelengths, favoring evolution to the kinetic Alfvén wave mode rather than the (fast) whistler mode.

Key words: solar wind – turbulence

Online-only material: color figures

1. INTRODUCTION

The inertial range of solar wind turbulence is comprised of a mixture of incompressible and compressible motions, with at least 90% of the energy due to the incompressible component (Bruno & Carbone 2005). If these fluctuations are interpreted as some mixture of the three MHD linear wave modes, then Alfvén waves are the dominant incompressible component, while slow and fast MHD waves make up the compressible component. These modes are distinguished by the correlation between the density and parallel magnetic field fluctuations: fast waves are positively correlated, slow waves are negatively correlated, and the density and parallel magnetic field fluctuations are both zero for Alfvén waves. As the wave amplitude is increased to nonlinear levels, even to the limit that they form discontinuities or shocks, these qualitative properties persist, corresponding to tangential and rotational discontinuities or fast and slow shocks (Baumjohann & Treumann 1996). The MHD limit of strong collisionality, however, is not valid in the solar wind; therefore, collisionless kinetic theory is necessary to determine the properties of the wave modes. Each of the kinetic versions of the MHD linear wave modes, determined using the Vlasov–Maxwell linear dispersion relation, retains the qualitative correlations between the density and parallel magnetic field fluctuation described above (Klein et al. 2012). In addition, these kinetic counterparts to the compressible modes may suffer damping from collisionless mechanisms (Barnes 1966).

Compressible fluctuations at inertial range scales λ in the solar wind (10^{-4} Hz $\lesssim f_{sc} \sim v_{sw}/\lambda \lesssim 1$ Hz; v_{sw} is the solar wind speed, f_{sc} is the Doppler-shifted frequency in the spacecraft frame) have been studied extensively, often interpreted as a mix of magnetoacoustic (fast MHD) waves and pressure-balanced structures (PBSs; Tu & Marsch 1995; Bruno & Carbone 2005). A PBS was first observed as an anti-correlation of thermal pressure and magnetic pressure at timescales of 1 hr (Burlaga & Ogilvie 1970), and subsequent investigations found a similar anti-correlation between the density and magnetic field magnitude (Vellante & Lazarus 1987; Roberts 1990). Theoretical studies of compressible MHD fluctuations in the low-Mach number, high-β limit interpreted these anti-correlated density–magnetic field strength observations as nonpropagating "pseudosound" density fluctuations (Matthaeus et al. 1991). A more comprehensive investigation confirmed the general density–magnetic field anti-correlation, but also identified a few positively correlated intervals consistent with the magnetosonic (fast MHD) wave (Tu & Marsch 1994). Numerical simulations suggested that the observed density–magnetic field intensity correlation at scales much larger than the inertial range is related to the large-scale structure of the heliospheric current sheet (Malara et al. 1996, 1997). Analysis of *Ulysses* observations found evidence for PBSs at inertial range scales in the high-latitude solar wind (McComas et al. 1995; Reisenfeld et al. 1999; Bavassano et al. 2004). Studies of the electron density up to $f_{sc} = 2.5$ Hz also found PBSs, but interpreted these as ion acoustic (slow MHD) waves, and recognized that PBSs are simply the ion acoustic (slow MHD) wave in the perpendicular wavevector limit (Kellogg & Horbury 2005). Recently, measurements of the anti-correlation between electron density and magnetic field strength indicated the existence of PBSs over timescales ranging from 10^3 s down to 10 s (Yao et al. 2011).

This Letter demonstrates that the compressible fluctuations in the inertial range are consistent with being due almost entirely to kinetic slow wave fluctuations, suggesting that little turbulent energy is transferred from large scales to whistler fluctuations below the ion gyroscale. First, we show that the density–magnetic field cross-correlation $C(\delta n, \delta B_\parallel)$ in the solar wind is $\simeq -1$ and increases slightly with ion plasma beta, β_i. Then we demonstrate excellent agreement with synthetic (eigenfunction) data in which less than 10% of the compressible energy is due to fast waves.

2. MEASUREMENTS

We use measurements from the magnetic field investigation (MFI; Lepping 1995) and the three-dimensional plasma (3DP) experiment (Lin 1995) on the *Wind* spacecraft, in the unperturbed solar wind at 1 AU, during the years 1994–2004. The magnetic field is sampled at either 11 or 22 vectors s^{-1} (depending on the spacecraft telemetry rate) then averaged down to the

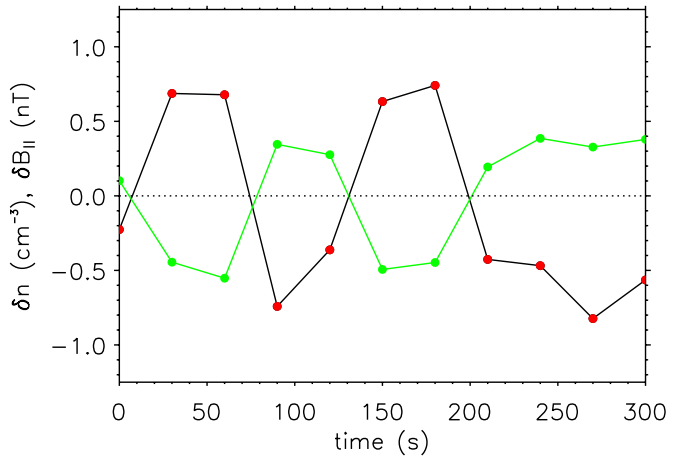

Figure 1. Example of waveforms of proton density fluctuations δn (black with red dots) and parallel magnetic field $\delta B_\parallel$ (green) fluctuations. This interval has $\langle \delta n \rangle_r \sim 0.6$ cm^{-3}, $\langle \delta B_\parallel \rangle_r \sim 0.4$ nT, and $C(\delta n, \delta B_\parallel) \sim -0.97$; however, even intervals with smaller density fluctuations exhibit significant anti-correlations.

(A color version of this figure is available in the online journal.)

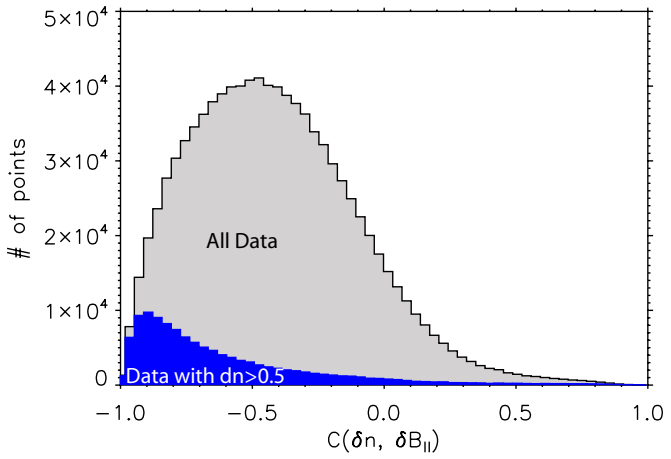

Figure 2. Histogram of the cross-correlations $C(\delta n, \delta B_\parallel)$ (gray, 1,089,491 points total) and those above the measurement noise threshold $\delta n > 0.5$ cm^{-3} (blue, 119,512 points total).

(A color version of this figure is available in the online journal.)

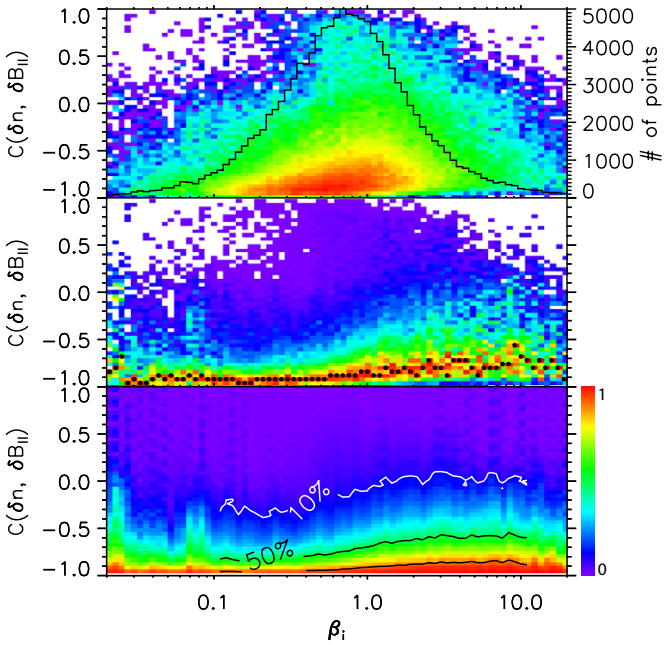

Figure 3. Upper: total distribution of the $C(\delta n, \delta B_\parallel)$ cross-correlation as a function of ion plasma beta β_i. The count in each β_i bin is overplotted (with the scale on the right). Middle: joint distribution of the $C(\delta n, \delta B_\parallel)$ cross-correlation normalized within each β_i bin. Black dots are the peak values in each β_i bin. Lower: cumulative distribution of $C(\delta n, \delta B_\parallel)$ with contours at 90%, 50%, and 10%. These distributions consist of 119,512 independent data intervals.

(A color version of this figure is available in the online journal.)

spacecraft spin period (3 s). The ion moments are computed on board the spacecraft at 3 s cadence; protons are separated from alpha particles by a fixed energy interval (which is occasionally adjusted in flight software) during the moment calculation; the solar wind alpha-particle abundance is typically 3%–5% of the proton number density. We select 1,089,491 300 s intervals of ambient solar wind data (corresponding to spatial intervals of approximately $L \approx 450$ km s^{-1} $\times$ 300 s $=$ 135,000 km $\sim$1350 ρ_i, where ρ_i is the ion Larmor radius) and the data are decimated by a factor of 10 (to 30 s cadence). Therefore, our data correspond to inertial range scales of approximately $k\rho_i \in (5 \times 10^{-3}, 5 \times 10^{-2})$. Since it has been shown that analyzing magnetized plasma turbulence with respect to the local mean magnetic field direction can illuminate features inaccessible using a globally computed field (Cho & Vishniac 2000), we compute the local mean field $\mathbf{B}_0$ by averaging the magnetic field data in 100 s windows. The fluctuation field $\delta\mathbf{B}$ is created by subtracting $\mathbf{B}_0$ and then is rotated to a field-aligned coordinate system defined by the $\mathbf{B}_0$ direction. In this new system, there is a compressible field fluctuation $\delta B_\parallel$ and shear components $\delta B_{\perp,1}$ and $\delta B_{\perp,2}$. The most probable amplitude of the shear component $\delta B_\perp = (\delta B_{\perp,1}^2 + \delta B_{\perp,2}^2)^{1/2}$ is approximately 3.4 times greater than most probable $\delta B_\parallel$ and corresponds to the Alfvénic component of the turbulence.

Proton density data $\delta n = n - n_0$ are detrended over the same time intervals. Proton density is an integral over the (3 s) distribution function $f(\mathbf{v})$, computed from particle flux measurements in 16 individual energy channels (Lin 1995). Since the counts are digitized discretely and the energy channels are also discrete (with $\Delta E/E \sim 0.2$), the 3DP proton density moments have a finite dynamic range. To assess this, we evaluated the joint probability distribution (not shown) of $\langle \delta n \rangle_r$ and $\langle \delta B_\parallel \rangle_r$, the rms values. Below values of $\langle \delta n \rangle_r \approx 0.5$ cm^{-3}, the joint pdf reverts from being well correlated to a broader set of values. Furthermore, the histogram of $\langle \delta n \rangle_r$ alone shows clearly an artificial (non-Poisson) lower cutoff at around this value, a cutoff not seen in $\langle \delta B_\parallel \rangle_r$. We take $\langle \delta n \rangle_r \approx 0.5$ cm^{-3} as the "noise" level of the density fluctuation measurement and restrict our analysis to intervals in which $\langle \delta n \rangle_r \geqslant 0.5$ cm^{-3}. This restriction reduces the data set from 1,089,491 to 119,512 data intervals and biases our sample to higher absolute densities. The most probable values of absolute density are $\sim$4 cm^{-3} for the full and $\sim$12 cm^{-3} for the thresholded data set. The distribution of plasma β_i is unaffected by the thresholding.

We compute the normalized, zero-lag cross-correlation $C(\delta n, \delta B_\parallel) = \langle \delta n \delta B_\parallel \rangle / \langle \delta n \rangle_r \langle \delta B_\parallel \rangle_r$, which has a range from -1 to 1. As described qualitatively above, we expect that $C(\delta n, \delta B_\parallel)$ will be negative (positive) for slow- (fast-) mode MHD fluctuations (see Figure 1). Figure 2 shows the distribution of $C(\delta n, \delta B_\parallel)$, both for all of the data and for the restricted data set that exceeds the density noise threshold $\langle \delta n \rangle_r \geqslant 0.5$ cm^{-3}. While the entire data set peaks below 0 (at $C(\delta n, \delta B_\parallel) \simeq -0.5$), the data set with well-resolved density amplitude levels peaks at $C(\delta n, \delta B_\parallel) \simeq -0.9$. Figure 3 shows the joint histogram of $C(\delta n, \delta B_\parallel)$ versus ion plasma beta β_i. The top panel shows

the distribution of points, with a histogram of β_i overplotted. The middle panel is the joint histogram normalized to number of β_i points in each β_i bin. This shows clearly that $C(\delta n, \delta B_\parallel)$ is near -1 over the entire interval, increasing slightly with β_i to $\simeq -0.7$ at $\beta_i = 10$. In the bottom panel, the cumulative distribution shows that fewer than 10% of the intervals have $C(\delta n, \delta B_\parallel) > 0$.

3. SYNTHETIC DATA

A cubic synthetic plasma volume spanning scales $3 \times 10^{-3} \leqslant k\rho_i \leqslant 4.8 \times 10^{-2}$ is constructed using a 32^3 grid. A spectrum of linear waves, with 90% of the energy in Alfvén waves and the remaining 10% in a mixture of kinetic fast and slow waves, consistent with the observed $k^{-5/3}$ one-dimensional energy spectrum of the magnetic field fluctuations $|\delta\mathbf{B}|$, is created in the volume using the linear eigenfunctions for these modes from the Vlasov–Maxwell linear dispersion relation (Quataert 1998; Howes et al. 2006). See Klein et al. (2012) for more details on the quasilinear premise of modeling plasma turbulence as a superposition of linear eigenfunctions, and note that alternative models for plasma turbulence have been suggested (Dmitruk & Matthaeus 2009; Parashar et al. 2010). A fully ionized proton and electron plasma is assumed, with isotropic Maxwellian velocity distributions, a realistic mass ratio $m_i/m_e = 1836$, equal ion and electron temperatures $T_i = T_e$, and non-relativistic conditions $v_{ti}/c = 10^{-4}$. Taking the MHD limit $k\rho_i \ll 1$, under these conditions the normalized linear Vlasov–Maxwell eigenfrequency depends on only two parameters, $\omega/(kv_A) = \overline{\omega}(\beta_i, \theta)$, the ion plasma beta β_i and the angle θ between the wavevector and the mean magnetic field (Klein et al. 2012). Once β_i has been chosen, one needs only to specify the distribution of energy in wavevector space. Compressible MHD turbulence simulations generate an isotropic distribution of fast waves and critically balanced distributions of Alfvén and slow waves (Cho & Lazarian 2003). Therefore, we initialize the fast wave energy isotropically, while the Alfvén and slow wave energy mimics a critically balanced distribution by setting all modes with $k_\parallel > k_0^{1/3} k_\perp^{2/3}$ to zero, where k_0 corresponds to the scale of the plasma volume.

Time series of density and parallel magnetic field fluctuations are constructed by sampling the synthetic data at a probe moving through the volume at an oblique angle with respect to the mean field (tests have confirmed insensitivity to the choice of angle). We then compute the cross-correlation $C(\delta n, \delta B_\parallel)$ as above. Figure 4 shows $C(\delta n, \delta B_\parallel)$ for several values of the ratio of fast wave energy to total compressible energy F versus ion plasma β_i. Peak histogram values (and FWHM error bars) are also shown. The solar wind data are in striking agreement with the synthetic data $F = 0.00$ curve. Note that if MHD eigenfunctions are used instead of the kinetic eigenfunctions, the synthetic $C(\delta n, \delta B_\parallel)$ curve does not fit the measured data (Klein et al. 2012).

To test the hypothesis that the observations may be simply explained by a mixture of Alfvénic fluctuations and PBSs, we have computed $C(\delta n, \delta B_\parallel)$ for the case where 90% of energy is in a critically balanced spectrum of Alfvén waves and 10% of the energy is in PBSs (red dashed). In this case, we find $C(\delta n, \delta B_\parallel) = -1$ for all values of β_i, in disagreement with the measured behavior.

4. DISCUSSION

Figure 4 shows that the observed correlation is consistent with a statistically negligible kinetic fast wave energy contribution

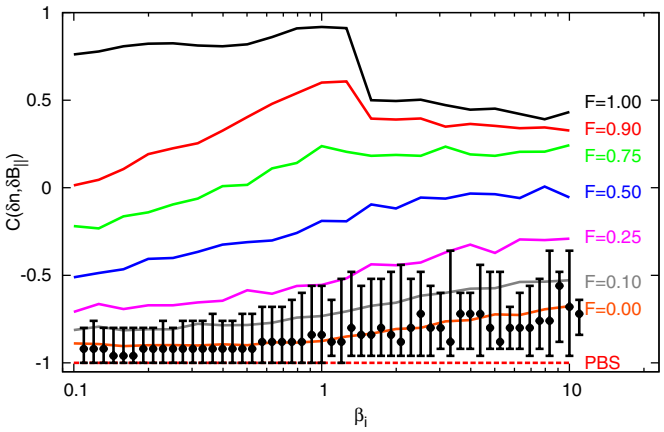

Figure 4. Comparison of measured values of the $C(\delta n, \delta B_\parallel)$ cross-correlation (black dots with FWHM error bars) to the synthetic data predictions for the ratio of kinetic fast wave to total compressible energy F. Best agreement is with $F = 0.00$, indicating that the compressible component of solar wind turbulence is almost entirely in the kinetic slow mode. A model with only Alfvén waves and PBSs (red dashed) predicts $C(\delta n, \delta B_\parallel) = -1$, which fails to reproduce the measured β_i dependence.

(A color version of this figure is available in the online journal.)

for the large sample used in this study. Note, however, that a very small fraction of the data intervals have a positive cross-correlation (see Figure 2), possibly indicating the presence of kinetic fast waves in these intervals. Another significant finding is that a model containing only Alfvénic turbulence and PBSs *cannot* explain the observations, as has been previously suggested in the literature.

Previous analyses have generally dismissed the possibility of kinetic slow waves because, in an isotropic Maxwellian plasma with warm ions, the collisionless damping via free streaming along the magnetic field is strong (Barnes 1966). However, in the limit $k_\perp \gg k_\parallel$ applicable to a critically balanced power distribution, the damping rate of the slow waves is proportional to the parallel component of the wavevector, $\gamma \propto k_\parallel$ (Howes et al. 2006). For exactly perpendicular wavevectors, the damping rate drops to zero—this perpendicular limit of the slow wave corresponds to an undamped, non-propagating PBS. In compressible, strong MHD turbulence, it has been shown that the slow modes are cascaded passively by the Alfvénic turbulence (Maron & Goldreich 2001; Schekochihin et al. 2009), so the energy cascade rate is related not to the slow wave frequency, but to the Alfvén wave frequency. Therefore, the more nearly perpendicular slow waves (possibly with $k_\parallel$ well below critical balance, $k_\parallel \ll k_0^{1/3} k_\perp^{2/3}$) may be cascaded to smaller scales on the timescale of the Alfvénic turbulence, while the collisionless damping of these modes remains weak.

We offer the following physical model of the compressible fluctuations in solar wind turbulence. At inertial range scales $k\rho_i \lesssim 0.1$, the density and parallel magnetic field fluctuations arise mainly from the kinetic counterparts of the fast and/or slow MHD waves. The measured $C(\delta n, \delta B_\parallel)$ cross-correlation at these scales strongly suggests that the compressible fluctuations are statistically dominated by kinetic slow mode fluctuations, and the distribution of power in wavevector space of these slow modes mimics the critically balanced distribution expected of Alfvénic fluctuations (Klein et al. 2012). These kinetic slow wave fluctuations may be cascaded as passive fluctuations to smaller scales by the Alfvénic turbulence (Maron & Goldreich 2001; Schekochihin et al. 2009), and so are predicted to exist

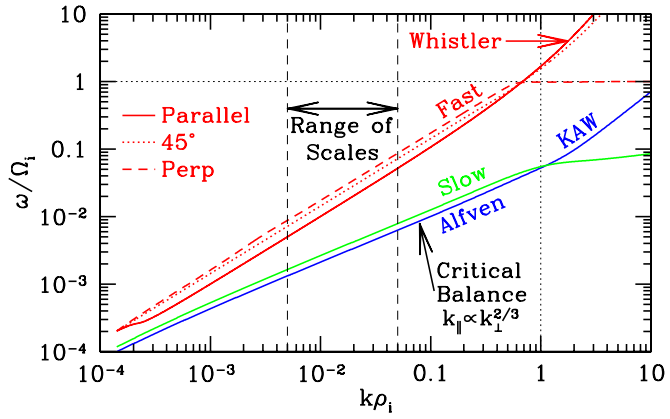

Figure 5. Plot of frequency ω/Ω_i vs. wavenumber $k\rho_i$ for the collisionless versions of the fast MHD (red), Alfvén (blue), and slow MHD (green) waves determined using the Vlasov–Maxwell linear dispersion relation. The range of scales considered in this study is indicated. Our measurements suggest that the solar wind spectrum lies on the blue–green curves.

(A color version of this figure is available in the online journal.)

down to the scale of the ion Larmor radius, and perhaps to even smaller scales. Thus, the evidence for PBSs over a range of timescales from 10^3 s to 10 s (Yao et al. 2011) is explained by the presence of a distribution of kinetic slow waves that is undergoing a turbulent cascade to smaller scales driven by the Alfvénic turbulence. In addition, these kinetic slow modes suffer collisionless damping at a rate $\gamma \propto k_\parallel$, meaning that the more perpendicular the wavevector, the slower the damping rate.

The lack of a statistically significant fast wave component in the inertial range of solar wind turbulence has implications for the cascade of energy to small scales. Because the nonlinear energy transfer in strong turbulence is believed to be dominated by local interactions in wavenumber space, significant nonlinear energy transfer occurs only between waves with similar linear frequencies. Figure 5 shows the real linear frequencies ω of the collisionless counterparts of the MHD fast, Alfvén, and slow waves as a function of $k\rho_i$. For the isotropically distributed fast waves (red), we plot the parallel (solid), 45° (dotted), and perpendicular (dashed) increase of the wavevector; slow (green) and Alfvén (blue) waves follow the critically balanced path $k_\parallel = k_0^{1/3} k_\perp^{2/3}$, with the isotropic driving scale $k_0\rho_i = 10^{-4}$ for all cases. Since only the fast wave turbulent cascade is expected to nonlinearly transfer energy to whistler waves at $k\rho_i \gtrsim 1$, our analysis suggests that there is little or no transfer of large-scale turbulent energy through the inertial range down to whistler waves at small scales.

Supported by NASA grants NNX10AC91G (Iowa) and NNX10AT09G (Berkeley) and by NSF grants AGS-1054061 (Iowa) and AGS-0962726 (Berkeley).

REFERENCES

Barnes, A. 1966, Phys. Fluids, 9, 1483
Baumjohann, W., & Treumann, R. A. 1996, Basic Space Plasma Physics (London: Imperial College Press)
Bavassano, B., Pietropaolo, E., & Bruno, R. 2004, Ann. Geophys., 22, 689
Bruno, R., & Carbone, V. 2005, Living Rev. Sol. Phys., 2, 4
Burlaga, L. F., & Ogilvie, K. W. 1970, Sol. Phys., 15, 61
Cho, J., & Lazarian, A. 2003, MNRAS, 345, 325
Cho, J., & Vishniac, E. T. 2000, ApJ, 539, 273
Dmitruk, P., & Matthaeus, W. H. 2009, Phys. Plasmas, 16, 062304
Howes, G. G., Cowley, S. C., Dorland, W., et al. 2006, ApJ, 651, 590
Kellogg, P. J., & Horbury, T. S. 2005, Ann. Geophys., 23, 3765
Klein, K. G., Howes, G. G., TenBarge, J. M., et al. 2012, ApJ, submitted
Lepping, R. 1995, Space Sci. Rev., 71, 207
Lin, R. P. 1995, Space Sci. Rev., 71, 125
Malara, F., Primavera, L., & Veltri, P. 1996, J. Geophys. Res., 101, 21597
Malara, F., Veltri, P., & Primavera, L. 1997, Phys. Rev. E, 56, 3508
Maron, J., & Goldreich, P. 2001, ApJ, 554, 1175
Matthaeus, W. H., Klein, L. W., Ghosh, S., & Brown, M. R. 1991, J. Geophys. Res., 96, 5421
McComas, D. J., Barraclough, B. L., Gosling, J. T., et al. 1995, J. Geophys. Res., 100, 19893
Parashar, T. N., Servidio, S., Breech, B., Shay, M. A., & Matthaeus, W. H. 2010, Phys. Plasmas, 17, 102304
Quataert, E. 1998, ApJ, 500, 978
Reisenfeld, D. B., McComas, D. J., & Steinberg, J. T. 1999, Geophys. Res. Lett., 26, 1805
Roberts, D. A. 1990, J. Geophys. Res., 95, 1087
Schekochihin, A. A., Cowley, S. C., Dorland, W., et al. 2009, ApJS, 182, 310
Tu, C.-Y., & Marsch, E. 1994, J. Geophys. Res., 99, 21481
Tu, C.-Y., & Marsch, E. 1995, Space Sci. Rev., 73, 1
Vellante, M., & Lazarus, A. J. 1987, J. Geophys. Res., 92, 9893
Yao, S., He, J.-S., Marsch, E., et al. 2011, ApJ, 728, 146